# Complete Mapping of the Stereochemical Course of Retentive Deprotonation/Alkylation of 1*H*-Benzo[*e*][1,4]diazepin-2(3*H*)-ones

Danny C. Hsu, Polo C.-H. Lam, Carla Slebodnick, and Paul R. Carlier*

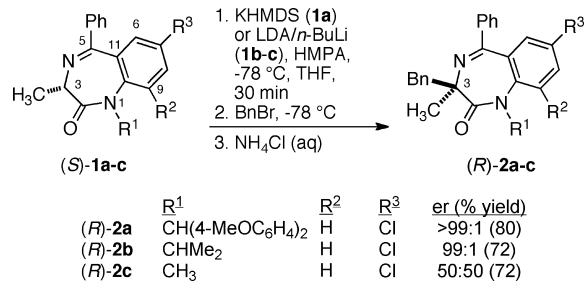*Department of Chemistry, Virginia Tech, Blacksburg, Virginia 24061*

Received September 4, 2009; E-mail: pcarlier@vt.edu

***Abstract:*** Enantiopure amino-acid derived 1*H*-benzo[*e*][1,4]diazepin-2(3*H*)-ones (BZDs) undergo highly retentive deprotonation/alkylation reactions. To confirm the role of stereolabile, axially chiral intermediates in these reactions and to determine the precise stereochemical course of deprotonation and alkylation, a new alanine-derived BZD (*S*)-**1d** was prepared. Because of slow diazepine ring inversion of the C3-alkylated derivatives of **1d**, it proved possible to determine that electrophiles react at the concave face of the enolate derived from **1d**. Furthermore, an enantiopure silyl enol ether derivative of (*S*)-**1d** was prepared and characterized by X-ray crystallography, confirming that deprotonation resulted in an (*M*)-configured axially chiral enolate. Activation parameters for diazepine ring inversion in the potassium enolate of **1d** were determined experimentally and are well-matched by density functional calculations. Finally, the factors leading to concave-face alkylation of the enolate derived from **1d** are analyzed based on calculated alkylation transition structures. Minimization of torsional effects at the BZD ring fusion and maximization of imine and amide resonance are proposed to favor concave-face alkylation.

## Introduction

The development of methods for the preparation of quaternary stereogenic centers in high enantioselectivity continues to receive considerable attention.[1] We have previously shown that enantiopure 1*H*-benzo[*e*][1,4]diazepin-2(3*H*)-ones (BZDs, e.g. **1a**−**b**) can be retentively functionalized at C3 by a deprotonation/alkylation sequence to afford the corresponding quaternary BZDs (e.g., **2a**−**b**, Scheme 1).[2−4] BZDs are well-known as privileged scaffolds in medicinal chemistry,[5−8] but prior to our work, very few examples containing quaternary stereogenic

**Scheme 1.** Effect of the N1 Substituent on the Deprotonation/Benzylation of Enantiopure BZDs (*S*)-**1a**−**c**



| | $R^1$ | $R^2$ | $R^3$ | er (% yield) |
|---|---|---|---|---|
| (*R*)-**2a** | CH(4-MeOC₆H₄)₂ | H | Cl | >99:1 (80) |
| (*R*)-**2b** | CHMe₂ | H | Cl | 99:1 (72) |
| (*R*)-**2c** | CH₃ | H | Cl | 50:50 (72) |

centers had been prepared.[9] The ability to prepare such compounds could further extend the usefulness of this scaffold.

To date, a key requirement for high stereoselectivity in the deprotonation/alkylation reactions depicted in Scheme 1 is the presence of a bulky substituent at N1; in these cases >98:2 er is typically attained.[2,4] If the N1 substituent is methyl, racemic products are obtained at −78 °C, as illustrated for (*S*)-**1c** (Scheme 1).[2] These observations and others led us to propose that success in these reactions depended on the formation of stereolabile, axially chiral enolates.[2−4,10,11] Enantioselective reactions that proceed through such intermediates have been described as examples of "memory of chirality."[2,3,10−20] Al-
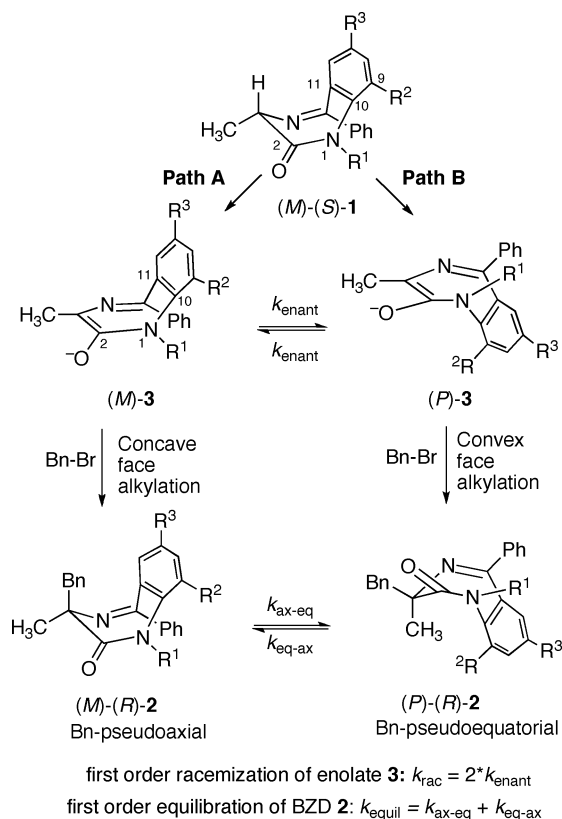
(1) Selected examples: (a) All carbon: Nojiri, A.; Kumagai, N.; Shibasaki, M. *J. Am. Chem. Soc.* **2009**, *131*, 3779–3784. Das, J. P.; Chechik, H.; Marek, I. *Nat. Chem.* **2009**, *1*, 128–132. Bui, T.; Syed, S.; Barbas, C. F., III. *J. Am. Chem. Soc.* **2009**, *131*, 8758–8759. May, T. L.; Brown, M. K.; Hoveyda, A. H. *Angew. Chem., Int. Ed.* **2008**, *47*, 7358–7362. (b) N-Substituted: Fu, P.; Snapper, M. L.; Hoveyda, A. H. *J. Am. Chem. Soc.* **2008**, *130*, 5530–5541. Fischer, D. E.; Xin, Z. Q.; Peters, R. *Angew. Chem., Int. Ed.* **2007**, *46*, 7704. (c) O-Substituted: Seto, M.; Roizen, J. L.; Stoltz, B. M. *Angew. Chem., Int. Ed.* **2008**, *47*, 6873–6876. Friel, D. K.; Snapper, M. L.; Hoveyda, A. H. *J. Am. Chem. Soc.* **2008**, *130*, 9942–9951.

(2) Carlier, P. R.; Zhao, H.; DeGuzman, J.; Lam, P. C.-H. *J. Am. Chem. Soc.* **2003**, *125*, 11482–11483.

(3) Carlier, P. R.; Lam, P. C.-H.; DeGuzman, J.; Zhao, H. *Tetrahedron: Asymmetry* **2005**, *16*, 2998–3002.

(4) Carlier, P. R.; Zhao, H.; MacQuarrie-Hunter, S. L.; DeGuzman, J. C.; Hsu, D. C. *J. Am. Chem. Soc.* **2006**, *128*, 15215–15220.

(5) Evans, B. E.; Rittle, K. E.; Bock, M. G.; DiPardo, R. M.; Freidinger, R. M.; Whitter, W. L.; Lundell, G. F.; Veber, D. F.; Anderson, P. S.; Chang, R. S. L.; Lotti, V. J.; Cerino, D. J.; Chen, T. B.; Kling, P. J.; Kunkel, K. A.; Springer, J. P.; Hirschfield, J. *J. Med. Chem.* **1988**, *31*, 2235–2246.

(6) Ellman, J. A. *Acc. Chem. Res.* **1996**, *29*, 132–143.

(7) Mishra, J. K.; Garg, P.; Dohare, P.; Kumar, A.; Siddiqi, M. I.; Ray, M.; Panda, G. *Bioorg. Med. Chem. Lett.* **2007**, *17*, 1326–1331.

(8) Butini, S.; Gabellieri, E.; Huleatt, P. B.; Campiani, G.; Franceschini, S.; Brindisi, M.; Ros, S.; Coccone, S. S.; Fiorini, I.; Novellino, E.; Giorgi, G.; Gemma, S. *J. Org. Chem.* **2008**, *73*, 8458–8468.

(9) Avdagic, A.; Lesac, A.; Majer, Z.; Hollosi, M.; Sunjic, V. *Helv. Chim. Acta* **1998**, *81*, 1567–1582.

(10) Zhao, H.; Hsu, D. C.; Carlier, P. R. *Synthesis* **2005**, 1–16.

(11) MacQuarrie-Hunter, S.; Carlier, P. R. *Org. Lett.* **2005**, *7*, 5305–5308.

(12) Kawabata, T.; Yahiro, K.; Fuji, K. *J. Am. Chem. Soc.* **1991**, *113*, 9694–9696.

(13) Fuji, K.; Kawabata, T. *Chem.—Eur. J.* **1998**, *4*, 373–376.

(14) Kawabata, T.; Suzuki, H.; Nagae, Y.; Fuji, K. *Angew. Chem., Int. Ed.* **2000**, *39*, 2155–2157.

**Scheme 2.** Possible Mechanisms (Path A and Path B) for Retentive Deprotonation/Benzylation of **1**



first order racemization of enolate **3**: $k_{rac} = 2 * k_{enant}$

first order equilibration of BZD **2**: $k_{equil} = k_{ax-eq} + k_{eq-ax}$

though this term still enjoys wide usage, we would point out that it is the *configuration* of the starting materials, not the *chirality* (i.e., mirror image nonsuperimposability), that is "memorized" in the intermediates of these reactions.[21] Leaving the terminology issue aside, we ask how does the retentive transformation from (*S*)-**1a** to (*R*)-**2a** occur? Two limiting mechanisms are presented in Scheme 2.

The nonplanarity of the diazepine ring of BZDs is well-known, and its conformation has traditionally been described with the (*M*)- or (*P*)- helical descriptors.[22,23] Furthermore, if the BZD bears a single substituent at C3, pseudoequatorial

(15) Kawabata, T.; Fuji, K. In *Topics in Stereochemistry*; Denmark, S. E., Ed.; John Wiley & Sons, Inc.: New York, 2003; Vol. 23, pp 175–205.
(16) Kawabata, T.; Matsuda, S.; Kawakami, S.; Monguchi, D.; Moriyama, K. *J. Am. Chem. Soc.* **2006**, *128*, 15394–15395.
(17) Kawabata, T.; Moriyama, K.; Kawakami, S.; Tsubaki, K. *J. Am. Chem. Soc.* **2008**, *130*, 4153–4157.
(18) Kolaczkowski, L.; Barnes, D. M. *Org. Lett.* **2007**, *9*, 3029–3032.
(19) Branca, M.; Gori, D.; Guillot, R.; Alezra, V.; Kouklovsky, C. *J. Am. Chem. Soc.* **2008**, 130.
(20) Branca, M.; Pena, S.; Guillot, R.; Gori, D.; Alezra, V.; Kouklovsky, C. *J. Am. Chem. Soc.* **2009**, *131*, 10711–10718.
(21) We have previously made this distinction in ref 4. We also commend Wolf's recent description of these reactions as examples of "self-regeneration of chiral elements with stereolabile intermediates" (Wolf, C. In *Dynamic Stereochemistry of Chiral Compounds: Principles and Applications*; Royal Society of Chemistry: Cambridge, UK, 2008; pp 282–289).
(22) Konowal, A.; Snatzke, G.; Alebic-Kolbah, T.; Kajfez, F.; Rendic, S.; Sunjic, V. *Biochem. Pharmacol.* **1979**, *28*, 3109–3113.
(23) We use the helical descriptors (*M*)- and (*P*)- to assign the sense of chirality of the ring, according to the sign of the C2N1C10C11 dihedral angle (*M* = minus, *P* = positive). This dihedral angle has the same sign as the C2C3N4C5 dihedral, which has historically (see ref 22) been used to describe the conformation of the BZD ring.

preference will cause an (*S*)-configured BZD (like (*S*)-**1**) to adopt the (*M*)-conformation.[22,24−27] With this necessary background established, (*M*)-(*S*)-**1** could undergo retentive deprotonation to give enolate (*M*)-**3** and subsequent concave-face benzylation to give (*M*)-(*R*)-**2** with the electrophile in the pseudoaxial position (Scheme 2, Path **A**). This pathway is attractive based on stereoelectronic considerations for deprotonation (i.e., alignment of the C3−H σ orbital with the C2 carbonyl π* orbital). However, an alternative mechanism would involve invertive deprotonation of (*M*)-(*S*)-**1** to (*P*)-**3** and convex-face benzylation to give (*P*)-(*R*)-**2**, this time featuring pseudoequatorial delivery of the incoming electrophile (Scheme 2, Path **B**). Although the invertive deprotonation of Path **B** seems unlikely, Kawabata has shown that, by judicious choice of amide base, it is possible to obtain either enantiomer of an axially chiral enolate from the same protected aminoacid ester.[16] Furthermore, on steric grounds, the convex-face benzylation of Path **B** appears favorable to the concave-face benzylation of Path **A**. In principle these pathways could be distinguished by determining the initial (*M*)- or (*P*)-conformation of the product (*R*)-**2**; however, up to now, fast conformational equilibration of the products **2** on the laboratory time scale[2,4,27,28] has precluded this approach (e.g., $t_{1/2}$(equil) = 2 s for **2b** at 298 K).[27] In this paper we report preparation of a new BZD substrate (*S*)-**1d** featuring C9-substitution (i.e., $R^2 \neq H$). Like (*S*)-**1a-b**, (*S*)-**1d** undergoes highly retentive deprotonation/alkylation reactions. However, conformational equilibration in quaternary derivatives of (*S*)-**1d** is slow enough to allow us to determine the initial disposition (pseudoaxial or pseudoequatorial) of the incoming electrophile. Furthermore, use of (*S*)-**1d** allowed us to capture an axially chiral BZD enolate intermediate in enantiopure form and determine its absolute configuration by X-ray crystallography. We are thus able to unambiguously determine the stereochemical course of both the BZD deprotonation and of the enolate alkylation reactions. Finally, computed enolate alkylation transition structures are examined to identify possible factors favoring concave-face alkylation.

## Synthetic and Mechanistic Studies

We noted above that success in retentive deprotonation/trapping reactions of BZDs **1** requires the presence of a large (i.e., 2°) substituent at N1. We envisioned this requirement to stem from the need to slow enantiomerization of the derived enolate **3** ($k_{enant}$, Scheme 2); calculations have shown closer contact of the N1 and C9 substituents ($R^1$ and $R^2$, respectively) in the ring inversion transition structures of **3b** and **3c** than in the ground state.[2] To further lower the rate of enantiomerization of the derived enolate ($k_{enant}$, Scheme 2), we prepared BZD (*S*)-**1d**, featuring methyl substitution at C9. As expected from the discussion above, X-ray crystallography of (*S*)-**1d** indicates a pseudoequatorial disposition of the methyl group (Figure 1A).[29] Thus (*S*)-**1d** adopts the (*M*)-conformation, as depicted in Scheme 2.

(24) Gilman, N. W.; Rosen, P.; Earley, J. V.; Cook, C.; Todaro, L. J. *J. Am. Chem. Soc.* **1990**, *112*, 3969–3978.
(25) Sunjic, V.; Lisini, A.; Sega, A.; Kovac, T.; Kajfez, F.; Ruscic, B. *J. Heterocycl. Chem.* **1979**, *16*, 757–761.
(26) Paizs, B.; Simonyi, M. *Chirality* **1999**, *11*, 651–658.
(27) Lam, P. C.-H.; Carlier, P. R. *J. Org. Chem.* **2005**, *70*, 1530–1538.
(28) Note that this rate is slow enough to allow both conformers to be resolved by ^{1}H NMR spectroscopy at room temperature (see refs 2–4).
(29) Crystallographic data (cif) are given in the Supporting Information and has been deposited as CCDC-696626 at the Cambridge Crystallographic Data Centre (www.ccdc.cam.ac.uk/data_request/cif).
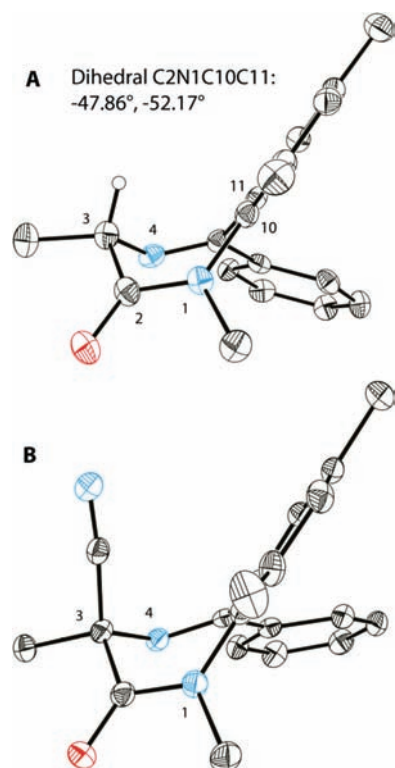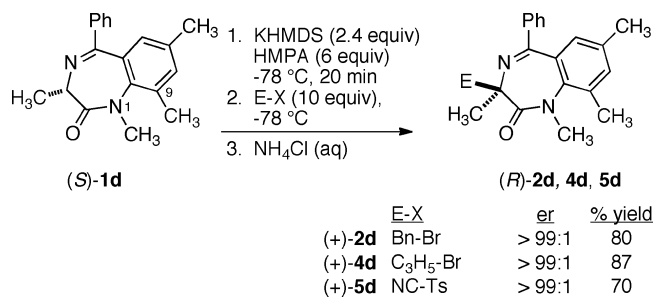
**Figure 1.** Anisotropic displacement ellipsoid drawings (50%) of (A) X-ray crystal structure of starting BZD (S)-**1d**, which adopts the (M)-conformation, and (B) X-ray crystal structure of cyanation product (R)-**5d**, demonstrating retentive substitution. Hydrogen atoms are omitted for clarity, except for C3-H in (S)-**1d**; note that, for this structure, only one of the two crystallographically independent molecules is shown.

**Scheme 3.** Deprotonation/Trapping Reactions of (S)-**1d**



|          | E-X                    | er      | % yield |
|----------|------------------------|---------|---------|
| (+)-**2d** | Bn-Br                | > 99:1  | 80      |
| (+)-**4d** | $C_3H_5$-Br          | > 99:1  | 87      |
| (+)-**5d** | NC-Ts                | > 99:1  | 70      |

Whereas **1c** ($R^1$ = Me, $R^2$ = H) gives racemic **2c** in a sequential deprotonation/benzylation protocol at −78 °C,[2] deprotonation/trapping of (S)-**1d** ($R^1$ = Me, $R^2$ = Me) at −78 °C gave C3-benzylated, -allylated, and -cyanated products in >99:1 er (**2d**, **4d**, **5d**, respectively, Scheme 3). These results are consistent with the idea that steric interaction between the $R^1$ and $R^2$ substituents governs the rate of enolate enantiomerization (Scheme 2). Retentive benzylation and allylation of (S)-**1d** are assumed based on precedent from analogues **1b**[2] and **1a**.[4] Retentive cyanation of (S)-**1d** (e.g., (R)-configuration) was confirmed by X-ray crystallography of (+)-**5d** (anomalous dispersion effects: see Supporting Information). X-ray crystallography of **5d**[30] also displayed a CN-axial conformation, which

---

(30) Crystallographic data (cif) and details on the use of anomalous dispersion effects to determine absolute configuration are given in the Supporting Information. This structure has also been deposited as CCDC-696624 at the Cambridge Crystallographic Data Centre (www.ccdc.ac.uk/data_request/cif).
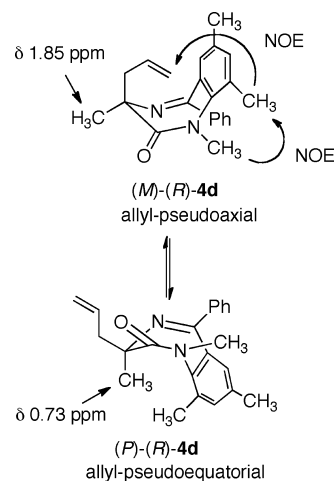
**Figure 2.** ^{1}H NMR chemical shift and [1]H−[1]H NOE assignments of allyl-pseudoaxial and pseudoequatorial conformers of (R)-**4d**.
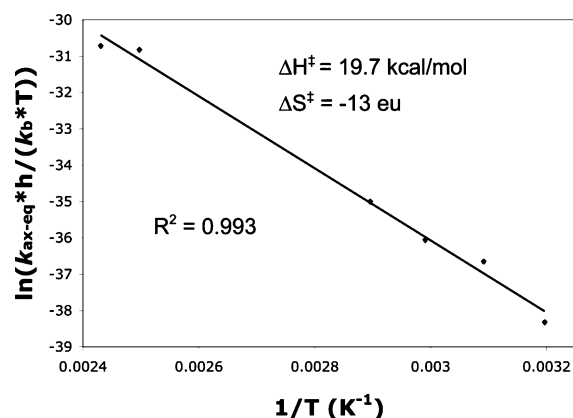


**Figure 3.** Eyring plot and activation parameters for conversion of allyl-pseudoaxial-**4d** to allyl-pseudoequatorial-**4d**.

was expected based on the small A-value of cyano relative to methyl (Figure 1B).[4] As expected, ^{1}H NMR spectroscopy (298 K, CDCl$_3$) of **2d** revealed a 57:43 mixture of the Bn-pseudoaxial and Bn-pseudoequatorial conformers. Similarly, **4d** appeared as a 53:47 mixture of allyl-pseudoaxial and allyl-pseudoequatorial conformers. Fortuitously the Bn-pseudoaxial and Bn-pseudoequatorial conformers of **2d** could be separated by column chromatography; separation of the conformers was also possible for **4d**. As we have described previously the conformers can be identified on the basis of chemical shift; [1]H−[1]H NOE correlations offered further conformation of the identity of allyl-pseudoaxial and allyl-pseudoequatorial **4d** (Figure 2).

The equilibration of isolated single conformers of **2d** and **4d** was followed by ^{1}H NMR spectroscopy (d$_6$-DMSO) at temperatures between 40 and 70 °C to determine the equilibration rate constants ($k_{equil}$ = $k_{ax-eq}$ + $k_{eq-ax}$ Scheme 2). Equilibration rate constants at higher temperatures (120 and 130 °C) were determined by [1]H−[1]H EXSY spectroscopy of the equilibrium mixtures.[27,31] From these studies we determined the activation parameters for ring inversion of the conformers of **2d** and **4d** (Figure 3 and Table 1). From these values we estimate equilibration half-lives ($t_{1/2}$(equil)) for **2d** and **4d** of 3.0 and 2.3 h at 25 °C respectively. These values are consistent with our observations made during chiral stationary phase HPLC of

---

(31) Perrin, C. L.; Dwyer, T. J. *Chem. Rev.* **1990**, *90*, 935−967.

***Table 1.*** Activation Parameters for Ring Inversion of Quaternary BZDs **2d** and **4d**

| BZD | direction | $\Delta H^{\ddagger}$ (kcal/mol)[a] | $\Delta S^{\ddagger}$ (eu)[a] |
|---|---|---|---|
| **2d** | ax-eq | 19.4 ± 0.9 (3) | −14 ± 3 (8) |
|  | eq-ax | 19.3 ± 0.9 (3) | −14 ± 3 (8) |
| **4d** | ax-eq | 19.7 ± 0.8 (2) | −13 ± 2 (7) |
|  | eq-ax | 19.5 ± 0.8 (2) | −13 ± 2 (7) |

[a] Values reported as mean ± standard error; 95% confidence limits are given in parentheses.
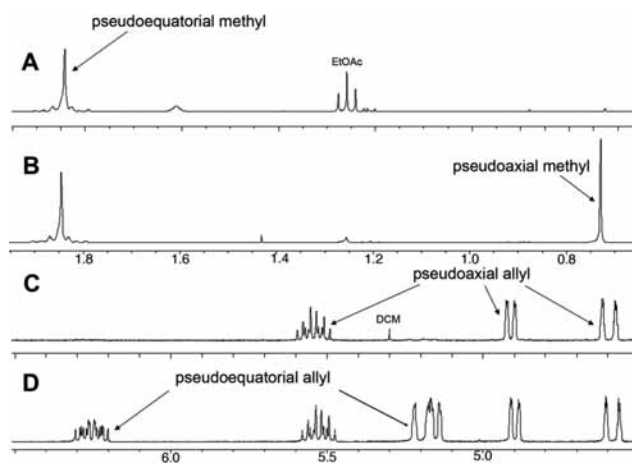


***Figure 4.*** (A) Methyl region of the ¹H NMR spectra of **4d** immediately following rapid, cold workup and chromatography; EtOAc represents residual ethyl acetate. (B) Methyl region of the ¹H NMR spectra of **4d** after storage under vacuum at room temperature. (C) Allyl region of the ¹H NMR spectra of **4d** immediately following rapid, cold workup and chromatography; DCM represents residual dichloromethane. (D) Allyl region of the ¹H NMR spectra of **4d** after storage under vacuum at room temperature.

these compounds. Unlike racemic **2a**−**c**, each of which gives two peaks (one for each enantiomer),[2,4] racemic **2d** gives four peaks on chiral stationary phase HPLC (two for each enantiomer; see Supporting Information). The same behavior is seen for racemic **4d**. With such slow conformational interconversion, it should be possible for us to ascertain which conformer is formed initially in deprotonation/trapping reactions of **1d**.

Thus we repeated the deprotonation/alkylation experiments depicted in Scheme 3, followed by a quick cold aqueous workup: TLC analysis at this point indicated formation only of the benzyl-pseudoaxial and allyl-pseudoaxial-products, respectively. Rapid flash chromatography with cold solvent, *in vacuo* concentration, and sample preparation were then performed: during this time the sample temperature never exceeded 5 °C (at this temperature calculated $t_{1/2}$(equil) = 34 and 27 h for **2d** and **4d** respectively). For both reactions, immediate ¹H NMR spectroscopic analysis confirmed a great predominance of the benzyl-pseudoaxial and allyl-pseudoaxial conformers of **2d** and **4d** respectively. After warming to room temperature, these samples gave the expected equilibrium mixture of conformers. Portions of the ¹H NMR spectra of the allylation experiment (i.e., **4d**) are shown in Figure 4.

After cold workup and chromatography only the pseudoequatorial methyl at δ 1.85 ppm is visible, but after equilibration at room temperature the pseudoaxial methyl group (δ 0.73 ppm) emerges (Figure 4A and 4B). Similarly, after cold workup only the signals for the pseudoaxial allyl group are visible, but after warming the signals for the pseudoequatorial allyl group appear (Figures 4C and 4D). These cold workup experiments clearly indicate pseudoaxial delivery of the electrophile. As such they
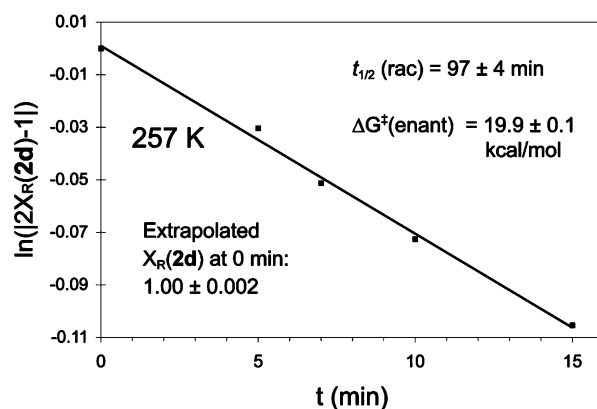


***Figure 5.*** Racemization of the enolate derived from (*S*)-**1d**. BZD (*S*)-**1d** was deprotonated with KHMDS (2.5 equiv) in THF with added HMPA (6 equiv) at −16 °C for a time *t*; benzyl bromide was added, and the enantiomer ratio of the product **2d** was determined (HPLC). $X_R$(**2d**) is the mole fraction of (*R*)-**2d**, and $|2X_R(\mathbf{2d}) - 1|$ is equivalent to the % ee of **2d** expressed as a number between 0 and 1.0. Based on the >99:1 er for **2d** measured at −78 °C (Scheme 3), $X_R$(**2d**) at *t* = 0 was set as 1.0.
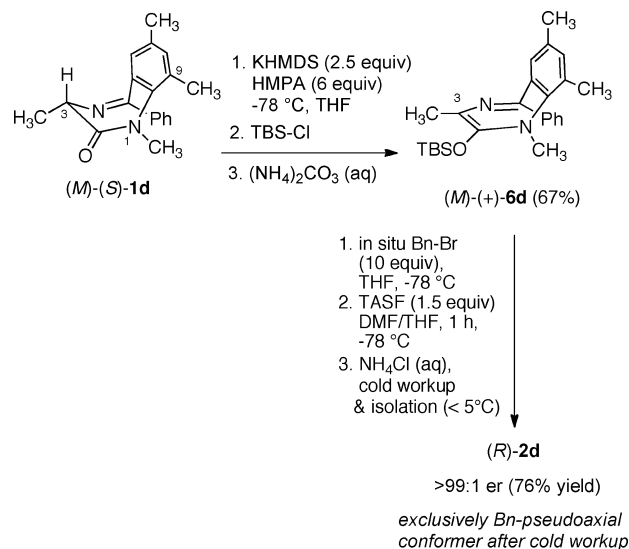
are consistent only with the Path **A** mechanism laid out in Scheme 2: deprotonation of (*S*)-**1d** to an (*M*)-configured enolate (e.g., (*M*)-**3d**) and concave-face alkylation (Path **A**, Scheme 2).

To gain further insight into the nature of the potassium enolate intermediate involved in these reactions, deprotonation/benzylation experiments were performed at 257 K, wherein the time *t* between additions of KHMDS and BnBr was varied from 5 to 15 min. Assuming a first-order mechanism, the rate of racemization $k_{rac}$ ($k_{rac} = 2*k_{enant}$) of the enolate intermediate can be determined from the slope of a plot of $\ln(|2X_R(\mathbf{2d}) - 1|)$ vs deprotonation time *t*.[3,14] In this manner we determined the racemization half-life ($t_{1/2}$(rac)) of the potassium enolate derived from **1d** to be 97 ± 4 min at 257 K, corresponding to an activation free energy for enantiomerization ($\Delta G^{\ddagger}$(enant)) of 19.9 ± 0.1 kcal/mol (Figure 5).

At 298 K we can estimate a $t_{1/2}$(rac) of 40 s for the potassium enolate of **1d**, assuming an entropy of activation of −10 eu (cf. $\Delta S^{\ddagger}$(enant) for **2d**, **4d**, Table 1). Thus despite the slow conformational inversion seen in the products **2d** and **4d**, the potassium enolate of **1d** would racemize rapidly at room temperature.

In the context of this facile room temperature enolate racemization, we attempted isolation of the corresponding silyl enol ether. After considerable experimentation, conversion of (*S*)-**1d** to the corresponding TBS enol ether **6d** was achieved in 67% yield (Scheme 4). Key to successful isolation of **6d** was the use of a mild basic quench and immediate trituration of crude **6d** with cold, dry $CH_3CN$; once isolated in this manner, **6d** proved quite stable. ¹H NMR spectroscopy of **6d** at 298 K indicated diastereotopic methyls at silicon, consistent with a chiral structure. To attempt determination of the coalescence temperature of the methyl groups, ¹H NMR spectra of **6d** were recorded at elevated temperatures. However, no line broadening was observed up to the decomposition point ($\Delta \nu = 11.2$ Hz, 130 °C, $d_6$-DMSO), indicating $\Delta G^{\ddagger}$(enant) > 21.6 kcal/mol. Recrystallization of **6d** from $CH_3CN$ allowed X-ray structure determination (Figure 6).[32]

The 1,4-diazepine ring of silyl enol ether **6d** adopts a chiral, sofa conformation with apparent $sp^2$ geometry at C3 and $sp^3$ geometry at N1 (Figure 6), similar to that calculated (B3LYP/6-31G*) previously for the enolate anions derived from **1b** and **1c**.[2] In addition, to our surprise, anomalous dispersion estab-

**Figure 7.** B3LYP/6-31G* structures and relative free energies (298 K) of (A) (*M*)-**6d$_A$**, the minimum energy equilibrium geometry of TBS enol ether (*M*)-**6d**, and (B) (*M*)-**6d$_A$***, the minimum energy ring inversion transition structure of TBS enol ether **6d**; the (*M*)-enantiomer is depicted arbitrarily.

lished that **6d** was present as a *single enantiomer*, exclusively in the (*M*)-conformation; in solution (*M*)-**6d** gave a sizable optical rotation ([α]$_D^{25}$ = +959, *c* = 1.85, CHCl$_3$). Enol ethers of axially chiral enolates have previously been isolated by Fuji and Kawabata, and their chirality and enantiomerization demonstrated by HPLC[12] and ^{1}H NMR.[14] However this is the first time that such a derivative has been isolated in enantiopure form and characterized by X-ray crystallography. Finally, (*M*)-**6d** proved useful as a precursor to a reactive enantiopure enolate. After surveying several desilylation reagents, we developed an optimized in situ desilylation/benzylation procedure using tris(dimethylamino)sulfonium difluorotrimethylsilicate (TASF) to generate the metal-free enolate at −78 °C in THF/DMF (Scheme 4). As expected, immediately following rapid cold workup (<5 °C) the sample of **2d** was shown by ^{1}H NMR spectroscopy to be exclusively in the Bn-pseudoaxial conformation; after column chromatography (*R*)-**2d** was isolated in 76% yield and >99:1 er.
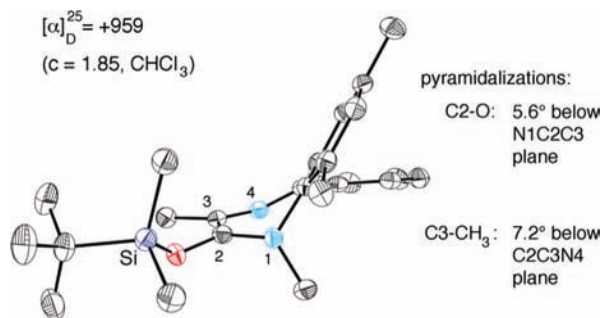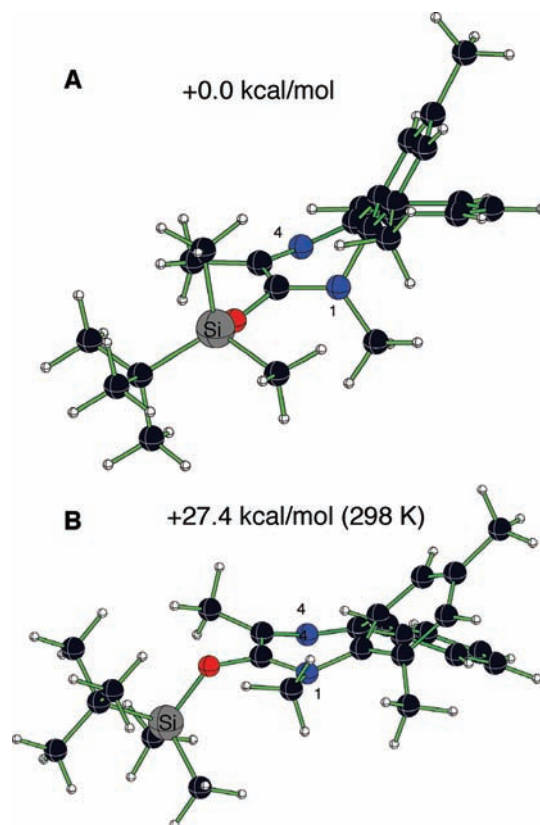


**Figure 6.** Anisotropic displacement ellipsoid drawings (50%) of (*M*)-(+)-**6d** (50% probability, hydrogens omitted for clarity).

## Computational Studies of Enol and Enolate Enantiomerization

The robust atropisomerism of TBS enol ether **6d** was unexpected in view of the short room temperature $t_{1/2}$(rac) we determined for the potassium enolate derived from **1d**. For comparison, Kawabata reported a very similar Δ*G*‡(enant) for the axially chiral TBS enol ether and potassium enolate derivatives of *N*-Boc-*N*-MOM pheny-

lalanine ethyl ester (16.8 and 16.0 kcal/mol respectively).[33] To estimate the barrier to enantiomerization of **6d**, its equilibrium geometries and ring inversion transition structures were located at B3LYP/6-31G*.[2,27,34] In total two diastereomeric equilibrium geometries (**6d$_A$**, **6d$_B$**) and two diastereomeric ring inversion transition structures (**6d$_A$***, **6d$_B$***) were located. These differ in the orientation of the TBS group relative to the puckered diazepine ring (i.e., above or below; see Supporting Information for details). Note that the calculated minimum energy equilibrium geometry (**6d$_A$**, Figure 7A) and X-ray structure of **6d** match quite well; an overlay of the seven diazepine ring atoms and the N1 and C3 methyl carbons gives an rmsd of only 0.043 Å.[35] The minimum energy ring inversion transition structure of **6d** (**6d$_A$***, Figure 7B) features a considerably flattened diazepine ring. As we have noted previously, ring inversion of BZDs (such as (*M*)-**6d**) could occur through either one of two enantiomeric transition structures;[2,27] thus the (*M*)-enantiomer of **6d$_A$*** is depicted arbitrarily in Figure 7B.

The calculated activation free energy for enantiomerization (Δ*G*‡(enant)) of **6d** is 27.4 kcal/mol (298 K), which gives a $t_{1/2}$(rac) of 80 days. This high calculated barrier is consistent with our ability to isolate (*M*)-**6d** in enantiopure form at room

(32) Crystallographic data (cif) and details on the use of anomalous dispersion effects to determine absolute configuration are given in the Supporting Information. The structure has also been deposited as CCDC-696625 at the Cambridge Crystallographic Data Centre (www.ccdc.cam.ac.uk/data_request/cif).

(33) Activation free energies of enantiomerization of 16.8 (356 K) and 16.0 (195 K) kcal/mol respectively were determined (see ref 14).

(34) Frisch M. J. et al. *Gaussian 03*, revision B.05; Gaussian, Inc.: Pittsburgh, PA, 2003.

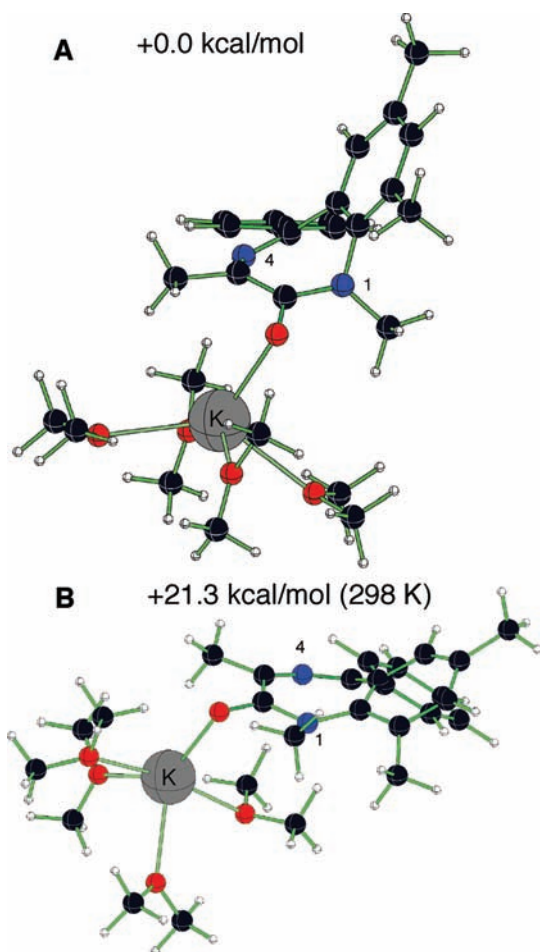(35) DeLano, W. L. *The PyMOL Molecular Graphics System* (2002) on http://www.pymol.org.

**A** +0.0 kcal/mol

**B** +21.3 kcal/mol (298 K)

**Figure 8.** B3LYP/6-31+G* structures and relative free energies of (A) (*M*)-**7d$_A$**, the minimum energy equilibrium geometry of tetrakis(dimethyl ether)-solvated potassium enolate (*M*)-**7d**, and (B) (*M*)-**7d$_A$**\*, the minimum energy ring inversion transition structures of tetrakis(dimethyl ether)-solvated potassium enolate **7d**; the (*M*)-enantiomer is depicted arbitrarily.

temperature, which suggests a barrier exceeding 26 kcal/mol (corresponding to a $t_{1/2}$(rac) > 7 days).

For comparison, we then located the equilibrium geometries and ring inversion transition structures of **7d**, the $K(OMe_2)_4^+$ salt of the enolate anion derived from **1d** (Figure 8).[36] Dimethyl ether was chosen as a THF surrogate for computational economy. Although the THF solvation number of the potassium enolate derived from **1d** is not known, tetrakis(Me$_2$O) solvates were easily located at B3LYP/6-31+G* and B3LYP/6-31G* and appeared to be the highest solvation state attainable. As was seen for TBS enol **6d** experimentally and computationally, the minimum energy equilibrium geometry (**7d$_A$**) of tetrakis(Me$_2$O)-solvated potassium enolate **7d** adopts a sofa conformation (Figure 8A). The corresponding minimum energy ring inversion transition structure (*M*)-**7d$_A$**\*, like (*M*)-**6d$_A$**\*, features a flattened diazepine ring (Figure 8B). The calculated $\Delta G^{\ddagger}$(enant) for **7d** of 21.3−21.5 kcal/mol (B3LYP/6-31+G* and B3LYP/6-31G* respectively, 257 K) is within 2 kcal/mol of the experimentally determined $\Delta G^{\ddagger}$(enant) for the potassium enolate derived from **1d** (a THF/HMPA solvate, Figure 5).

For reference we also calculated the equilibrium geometry of the enolate free ion **3d** and its ring inversion transition structure **3d**\* (B3LYP/6-31+G* and B3LYP/6-31G*; see Supporting Infor-

---

(36) Two diastereomeric equilibrium geometries (**7d$_A$**, **7d$_B$**) and three diastereomeric ring inversion transition structures (**7d$_A$**\*, **7d$_B$**\*, **7d$_C$**\*) were located. These differ in the orientation of the solvated potassium relative to the puckered diazepine ring (i.e. above, roughly in plane, or below); see Supporting information for details.

---

**Chart 1.** Bicyclic Lactams Whose Enolates Favor Concave-Face Alkylation[a]



8  9a: R = Ph  9b: R = *i*-Pr  9c: R = *t*-Bu  10

11  12  13
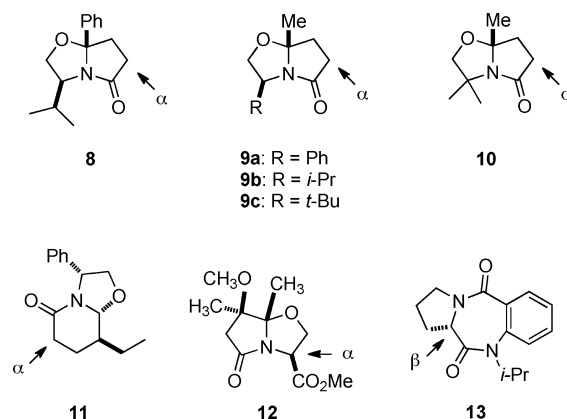
[a] The position and preferred face (α or β) of alkylation are indicated by each arrow.

mation). These structures are quite similar to those calculated for **6d** and **7d**, and the calculated $\Delta G^{\ddagger}$(enant) values of 21.0 and 20.1 kcal/mol (B3LYP/6-31+G* and B3LYP/6-31G* respectively, 257 K) of **3d** are slightly lower than those calculated for the $K(OMe_2)_4^+$ salt **7d**. The similarity in $\Delta G^{\ddagger}$(enant) for **3d** and **7d** suggests that the $K(OMe_2)_4^+$ fragment poses little steric hindrance in the enantiomerization transition structure. How can the significantly higher enantiomerization barrier of TBS enol **6d** then be rationalized? This difference (6−7 kcal/mol) does not appear to be a consequence of greater steric hindrance in the TBS enol, since the closest contact of TBS methyl carbons with the N1 and C3 Me carbon atoms in **6d**\* exceeds 3.3 Å. It is possible that electronic factors play a role in the higher enantiomerization barrier of **6d** relative to that of **3d** and **7d**.

## Discussion of Factors Contributing to the Observed Selectivity for Concave-Face Alkylation

What factors are responsible for the apparently contra-steric concave-face alkylation of the enolate derived from **1d**? Concave-face alkylation of enolates derived from bicyclic lactams is well-known in the work of Meyers (e.g., **8**,[37] **9a−c**,[38] **10**,[39] Chart 1) and has been observed in related systems by other investigators (**11**,[40] **12**[41]).

We have also observed concave-face alkylation in reactions of the conformationally locked proline-derived 3,4-dihydro-1*H*-benzo[*e*][1,4]diazepine-2,5-diones **13**.[4,11] The factors controlling diastereofacial selectivity of cyclic enolates has received considerable computational scrutiny, and several nonsteric factors have been proposed to contribute to these selectivities. In the case of Meyers-type enolates, concave selectivity has been attributed to the orientation of the amide N lone pair[42] and the position of the metal cation.[43] However, analysis of calculated alkylation transition structures of Meyers-type enolates casts

---

(37) Meyers, A. I.; Harre, M.; Garland, R. *J. Am. Chem. Soc.* **1984**, *106*, 1146–1148.

(38) Romo, D.; Meyers, A. I. *Tetrahedron* **1991**, *47*, 9503–9569.

(39) Meyers, A. I.; Seefeld, M. A.; Lefker, B. A.; Blake, J. F.; Williard, P. G. *J. Am. Chem. Soc.* **1998**, *120*, 7429–7438.

(40) Amat, M.; Escolano, C.; Lozano, O.; Llor, N.; Bosch, J. *Org. Lett.* **2003**, *5*, 3139–3142.

(41) Aydillo, C.; Jimenez-Oses, G.; Busto, J. H.; Peregrina, J. M.; Zurbano, M. M.; Avenoza, A. *Chem.—Eur. J.* **2007**, *13*, 4840–4848.

(42) Meyers, A. I.; Seefeld, M. A.; Lefker, B. A.; Blake, J. F. *J. Am. Chem. Soc.* **1997**, *119*, 4565–4566.

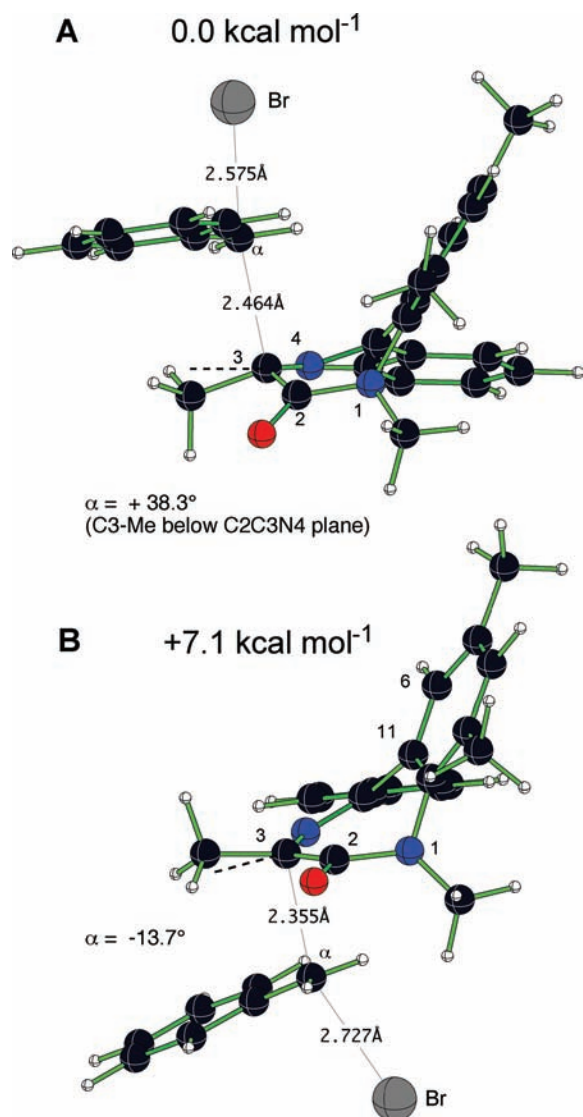(43) Ikuta, Y.; Tomoda, S. *Tetrahedron Lett.* **2003**, *44*, 5931–5934.

## A    0.0 kcal mol$^{-1}$



α = + 38.3°
(C3-Me below C2C3N4 plane)

## B    +7.1 kcal mol$^{-1}$



α = -13.7°

**Figure 9.** Minimum energy B3LYP/6-31G* transition structures for benzyl bromide alkylation of enolate anion (*M*)-**3d**. (A) concave-face alkylation transition structure *concave*-(*M*)-**2d***; (B) convex-face alkylation transition structure *convex*-(*M*)-**2d***. Relative free energies (195 K) are calculated at B3LYP/6-31+G*//B3LYP/6-31G*. Pyramidalization α represents deformation (deg) of C3-Me below (+) or above (−) the C2C3N4 plane.

doubt on the generality of the amide N lone pair effect[39] and suggests that minimization of torsional strain plays a crucial role.[44] Minimization of torsional strain has also been implicated in the concave-selective alkylations of **11**.[45] In the case of bicyclic lactams **12** and **13**, alkylation facial selectivity was observed to match the calculated pyramidalization[46−48] at the reactive center in the corresponding metal enolates.[11,41] Such a correlation was first noted by Seebach, who characterized imidazolidinone TBS enols by X-ray crystallography.[48]

(44) Ando, K.; Green, N. S.; Li, Y.; Houk, K. N. *J. Am. Chem. Soc.* **1999**, *121*, 5334–5335.
(45) Soteras, I.; Lozano, O.; Gomez-Esque, A.; Escolano, C.; Orozco, M.; Amat, M.; Bosch, J.; Luque, F. J. *J. Am. Chem. Soc.* **2006**, *128*, 6581–6588.
(46) Rondan, N. G.; Paddon-Row, M. N.; Caramella, P.; Houk, K. N. *J. Am. Chem. Soc.* **1981**, *103*, 2436–2438.
(47) Seebach, D.; Zimmerman, J.; Gysel, U.; Ziegler, R.; Ha, T.-K. *J. Am. Chem. Soc.* **1988**, *110*, 4763–4772.
(48) Seebach, D.; Maetzke, T.; Petter, W.; Klötzer, B.; Plattner, D. A. *J. Am. Chem. Soc.* **1991**, *113*, 1781–1786.

**Table 2.** B3LYP/6-31+G*//B3LYP/6-31G* Relative Free Energies and Selected Contact Distances of Concave- And Convex-Alkylation Transition Structures



*concave*-(*M*)        *convex*-(*M*)

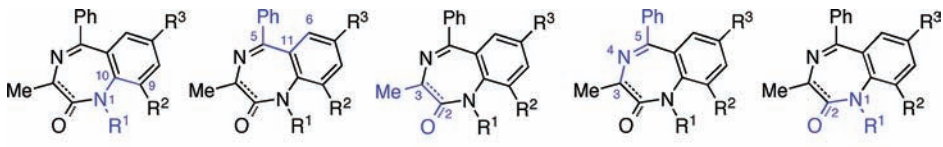| Structure | R$^1$ | R$^2$ | R$^3$ | R$^4$ | Rel G(195) (kcal/mol) | C3−Cα (Å) | R$^1$−Cα closest contact (Å)[a] |
|---|---|---|---|---|---|---|---|
| *concave*-(*M*)-**2d*** | Me | Me | Me | Ph | 0.0 | 2.464 | 5.076 |
| *convex*-(*M*)-**2d*** | Me | Me | Me | Ph | 7.1 | 2.355 | 3.642 |
| *concave*-(*M*)-**4d*** | Me | Me | Me | vinyl | 0.0 | 2.445 | 4.955 |
| *convex*-(*M*)-**4d*** | Me | Me | Me | vinyl | 8.6 | 2.334 | 3.617 |
| *concave*-(*M*)-**2b*** | i-Pr | H | Cl | Ph | 0.0 | 2.421 | 5.124 |
| *convex*-(*M*)-**2b*** | i-Pr | H | Cl | Ph | 4.4 | 2.351 | 3.648 |

[a] Distances were measured to the closest carbon atom of the R$^1$ group; in most cases this was the atom attached to N1.

Close inspection of the X-ray structure of our TBS enol (+)-**6d** does reveal a slight pyramidalization (α) of C3 (Figure 6). This deformation places the C3 methyl group 7.2° below the plane defined by C2C3N4, so as to orient a virtual sp$^3$ orbital toward the concave-face and preferred alkylation trajectory (Figure 6). Note that the deformation seen in the X-ray structure of **6d** is maintained in the B3LYP/6-31G* equilibrium geometries of TBS enol **6d** (9.1°), enolate anion **3d** (15.1°), and K(OMe$_2$)$_4^+$ salt **7d** (13.6°). Note further that this deformation does not reduce torsional strain with the C2-oxygen, because C2 has the same sense of pyramidalization. In the X-ray structure of (*M*)-**6d**, the C2-oxygen is 5.6° below the N1C2C3 plane, nearly eclipsing the methyl (O−C2−C3−Me dihedral angle = +5.1°). How does the C3 pyramidalization seen in the X-ray structure of **6d** relate to the observed concave-face alkylation? Following Houk[46] and Seebach[47] we believe that pyramidalization does not in itself dictate stereoselectivity but rather reflects interactions in the ground state that have larger energetic consequences in the transition states.

We thus undertook computational studies of the competing concave- and convex-face alkylation transition structures. Although it is clear that the reactive enolate species may not be monomeric,[49] computational resource limitations restricted our studies to monomers. Our decision to study alkylation of the free enolate anion **3d** (rather than metal salts) was motivated principally by our observation that identically high enantioselectivity was observed with both the potassium and tris(dimethylamino)sulfonium enolates (cf. Schemes 3 and 4). Thus it seemed likely that facial selectivity derived from the cyclic enolate itself, rather than from interaction with two disparate cations.

Minimum energy B3LYP/6-31G* transition structures *concave*-(*M*)-**2d*** and *convex*-(*M*)-**2d*** for benzyl bromide alkylation of the enolate free anion **3d** were located at B3LYP/6-31G* (Figure

(49) Seebach, D. *Angew. Chem., Int. Ed.* **1988**, *27*, 1624–1654.

***Table 3.*** C3 Pyramidalizations (α) and Selected Dihedral Angles for X-ray Structures (**1d**, **5d**) and Computed (B3LYP/6-31G*) Equilibrium Geometries (**7d**, **3d**) and Transition Structures (**2d\***, **4d\***, **2b\***)



| structure[a] | origin | diazepine conformation | pyramidalization α (deg)[c] | R¹N1C10C9 (deg) | C6C11C5Ph (deg) | MeC3C2O (deg) | C3N4C5Ph (deg) | R¹N1C2O (deg) |
|---|---|---|---|---|---|---|---|---|
| *concave*- (*M*)-**2d\*** | calc[b] | incipient boat | 38.3 | −50.8 | 41.5 | −2.0 | 173.8 | 16.3 |
| *convex*- (*M*)-**2d\*** | calc[b] | sofa | −13.7 | −45.9 | 36.7 | 17.7 | 170.8 | 30.1 |
| *concave*- (*M*)-**4d\*** | calc[b] | incipient boat | 37.3 | −51.1 | 40.7 | −0.6 | 173.5 | 15.6 |
| *convex*- (*M*)-**4d\*** | calc[b] | sofa | −14.3 | −45.5 | 37.3 | 17.0 | 170.9 | 31.0 |
| *concave*- (*M*)-**2b\*** | calc[b] | incipient boat | 38.3 | −40.9 | 36.7 | −4.2 | 174.1 | 11.4 |
| *convex*- (*M*)-**2b\*** | calc[b] | sofa | −14.2 | −40.6 | 36.4 | 17.3 | 171.1 | 30.1 |
| (*M*)-**7d**$_A$ | calc[b] | sofa | 13.6 | −53.2 | 37.0 | 15.0 | 172.1 | 18.5 |
| (*M*)-**3d** | calc[b] | sofa | 15.1 | −51.4 | 35.4 | 6.5 | 169.3 | 19.3 |
| (*M*)-(*S*)-**1d** | X-ray | boat | 53.6, 54.8[d] | −57.1, −53.0[d] | 50.4, 43.2[d] | 16.2, 14.5[d] | 176.7, 179.9[d] | 8.0, 6.3[d] |
| (*M*)-(*R*)-**5d** | X-ray | boat | 57.3 | −53.3 | 47.4 | 8.7 | 178.9 | 4.9 |

[a] As in Table 2, the electrophile in transition structures **2d\*** and **2b\*** is BnBr, and the electrophile in transition structures **4d\*** is allyl bromide. [b] Calculated geometry at B3LYP/6-31G*. [c] As in Figures 6 and 9, pyramidalization α represents the deformation (deg) of C3-Me below (+) or above (−) the C2C3N4 plane. [d] As noted in Figure 1, there are two molecules in the unit cell of (*M*)-(*R*)-**1d**.

9). Consistent with our experimental results, a significant preference (7.1 kcal/mol at B3LYP/6-31+G*//B3LYP/6-31G*, 195 K) is seen for concave-face benzylation (**A**, Figure 9). Competing concave- and convex-face transition structures were also located for allylation of enolate **3d** (e.g., **4d\***) and benzylation of enolate **3b** (**2b\***; see Supporting Information for structure diagrams). Significant concave-face preferences are also seen in each case (Table 2: 8.6 and 4.4 kcal/mol, respectively).

Thus density functional calculations reproduce the observed retentive outcome of deprotonation/alkylation reactions of (*S*)-**1b** and **1d** (Schemes 1, 3). Intermolecular contact distances in the calculated transition structures also suggest that the lower energy concave-face alkylation transition structures are sterically disadvantaged. The forming C3−Cα bond in the concave-face transition structures is 0.07 to 0.11 Å longer than those in the corresponding convex-face structures (Figure 9A and B, Table 2), suggesting greater steric hindrance[50−52] for concave-face attack. Unfavorable steric interaction between Cα of the electrophile and the N1 substituent (i.e., R¹) during convex-face alkylation can also be ruled out. A review of all the alkylation transition structures shows that the shortest contact between the electrophile and R¹ of the convex alkylation transition structures is never less than 3.6 Å (Table 2). Thus intermolecular steric interactions do not seem to control the alkylation facial selectivity.

The most striking feature of the alkylation transition structures to emerge from Figure 9 is the incipient boat conformation of *concave*-(*M*)-**2d\***. As shown in Figure 9A, *concave*-(*M*)-**2d\*** features a 38.3° pyramidalization (α) at C3, significantly greater than that seen in the TBS enol **6d** and approaching that seen in the X-ray structures of BZDs **1d** and **5d** (53.6° to 57.3°, Table 3). Alkylation transition structures *concave*-(*M*)-**4d\*** and -**2b\*** also adopt incipient boat conformations and feature C3 pyra-

midalizations (α) of 37.3° and 38.3° (Table 3). In contrast, *convex*-(*M*)-**2d\***, -**4d\***, and -**2b\*** retain a sofa conformation and feature inverted pyramidalizations at C3 (α = −13.7° to −14.3°; Figure 9B, Table 3).

We propose that the difference in energy of the concave- and convex-face alkylation transition structures stems from the conformational preferences of the BZD ring system. We would note that 1,4-diazepines, like cycloheptatriene,[53] have only one conformation (the boat). From the X-ray crystal structures of BZDs (*M*)-(*S*)-**1d** and (*M*)-(*R*)-**5d** (Figure 1) it is evident how the boat conformation minimizes torsional strain and maximizes π overlap in the amide and imine functional groups. In particular, in (*M*)-(*S*)-**1d** and (*M*)-(*R*)-**5d** dihedral angles at the ring fusion are large: R¹N1C10C9 ranges from −53.0° to −57.1°, and C6C11C5Ph ranges from 43.2° to 50.4° (Table 3). The dihedral angle MeC3C2O (which adjoins the forming C3−Cα bond) is small but not eclipsed (8.7° to 16.2°, Table 3). Finally, N4−C5 π overlap in the imine is maximized by C3N4C5Ph dihedral angles ranging from 176.7° to 179.9°, and N1−C2 π overlap in the amide is maximized by R¹N1C2O dihedral angles ranging from 4.9° to 8.0° (Table 3).

As we review these dihedral angles in the concave- and convex-alkylation transition structures, some advantageous features of concave-face alkylation begin to emerge. In particular when comparing the dihedral angles at the ring fusion (R¹N1C10C9 and C6C11C5Ph), the values in *concave*-(*M*)-**2d\*** are ~5° larger than those at *convex*-(*M*)-**2d\***. Similarly, as evidenced by the C3N4C5Ph dihedral angle, π overlap in the imine is slightly better in *concave*-(*M*)-**2d\*** relative to *convex*-(*M*)-**2d\***. The most striking dihedral angle difference between concave- and convex-(*M*)-**2d\*** is seen along R¹N1C2O (16.3° and 30.1°, respectively, Table 3), signaling decreased amide π overlap in convex-(*M*)-**2d\***. These same differences in dihedral angles are also seen in the allylation transition structures *concave*- and *convex*-(*M*)-**4d\*** (Table 3). For *concave*- and

(50) Jensen, F. *Chem. Phys. Lett.* **1992**, *196*, 368–376.
(51) Streitwieser, A.; Choy, G. S.-C.; Abu-Hasanayn, F. *J. Am. Chem. Soc.* **1997**, *119*, 5013–5019.
(52) Mohamed, A. A.; Jensen, F. *J. Phys. Chem. A* **2001**, *105*, 3259–3268.
(53) Eliel, E. L.; Wilen, S. H.; Mander, L. N. In *Stereochemistry of Organic Compounds*; Wiley-Interscience: New York, 1994, p 764.

*convex*-(*M*)-**2b***, better imine and amide $\pi$ overlap is seen in the *concave*-alkylation transition structure (Table 3). The absence of significant differences in the ring fusion dihedrals (R$^1$N1C10C9 and C6C11C5Ph) for *concave*- and *convex*-(*M*)-**2b*** may correlate to the lower predicted $\Delta\Delta G^{\ddagger}$ relative to **2d*** (4.4 vs 7.1 kcal/mol, Table 2). Finally we would note that, unexpectedly, torsional strain along MeC3C2O appears to be more significant in the concave-alkylation transition structures than in the convex-alkylation transition structures. Thus overall, the preference for concave-face alkylation appears to correlate best to better $\pi$-overlap (amide and imine) and reduced torsional strain at the ring fusion in the concave-face alkylation transition structures.

## Conclusions

Reactions involving stereolabile, axially chiral intermediates can offer excellent enantioselectivity but present intriguing mechanistic questions. How is stereochemical information transferred from the configuration of the starting material to a chiral axis of the intermediate and then back to the reconstituted stereogenic center of the product? In the case of retentive deprotonation/alkylation of BZD (*S*)-**1d**, we established that deprotonation stereoselectively generates an (*M*)-configured enolate, by X-ray crystallographic characterization of TBS enol (*M*)-**6d**. Furthermore, we demonstrated that the alkylation of the enolate derived from **1d** occurs on the concave side. Finally, BZD enolate alkylation was studied computationally by locating pairs of concave- and convex-face alkylation transition structures. Despite apparent greater steric hindrance, concave-face alkylation minimizes torsional effects at the BZD ring fusion and maximizes imine and amide resonance.

JA907507J